International Journal of Heat and Mass Transfer 196 (2022) 123230

Contents lists available at ScienceDirect

International Journal of Heat and Mass Transfer

journal homepage: www.elsevier.com/locate/hmt

Energy integral equation for premixed flame-wall interaction in turbulent boundary layers and its application to turbulent burning velocity and wall flux evaluations

Sanjeev Kr. Ghai [a], Umair Ahmed [a], Markus Klein [b,*], Nilanjan Chakraborty [a]

[a] School of Engineering, Newcastle University, Claremont Road, Newcastle upon Tyne NE1 7RU, UK
[b] Department of Aerospace Engineering, University of the Bundeswehr Munich, Werner-Heisenberg-Weg 39, Neubiberg 85577, Germany

ARTICLE INFO

Article history:
Received 11 April 2022
Revised 18 June 2022
Accepted 10 July 2022
Available online 21 July 2022

Keywords:
Energy conservation equation
Premixed V-flame-wall interaction
Turbulent boundary layer
Wall heat flux
Turbulent burning velocity

ABSTRACT

An integral form of the energy conservation equation has been derived from the first principle for low Mach number conditions for statistically steady premixed flame-wall interaction within turbulent boundary layers. The validity of this equation has been demonstrated based on three-dimensional Direct Numerical Simulation data of statistically stationary oblique quenching of a turbulent premixed V-shaped flame in a channel flow configuration as a result of its interaction with an inert isothermal wall. It has been found that the wall heat flux and the integral of chemical heat release in the wall normal direction within the turbulent thermal boundary layer are the major contributors in the energy integral equation, and their difference is accounted for by the advection contribution. The magnitudes of the wall heat flux increase, and integral of heat release rate across the thermal boundary layer decrease with increasing distance from the leading edge of the boundary layer as a result of flame quenching. The integral form of the energy conservation equation has been utilised to demonstrate that the Nusselt number (or Stanton number) for wall heat transfer is intrinsically related to the turbulent burning velocity in the case of flame-wall interaction within turbulent boundary layers. A Flame Surface Density based reaction rate closure, modified to account for the near-wall behaviour, has been utilised to estimate the mean Nusselt number in the case of flame-wall interaction within turbulent boundary layers, which revealed that the modelling limitations of the mean reaction rate closure may give rise to inaccuracies in the estimation of the mean Nusselt number. By contrast, the measurements of mean velocity, temperature, and wall heat flux can be utilised to estimate the turbulent burning velocity within the turbulent boundary layer using the newly derived energy integral equation.

© 2022 The Author(s). Published by Elsevier Ltd.
This is an open access article under the CC BY-NC-ND license
(http://creativecommons.org/licenses/by-nc-nd/4.0/)

1. Introduction

Flame-Wall Interaction (FWI) in turbulent boundary layers (TBLs) plays a pivotal role in the development of clean, fuel-efficient engine technologies across all transportation sectors in response to the call for combating climate change. Many industrial combustors are currently being redesigned for their use with electric powertrains beyond 2035 [1]. To date, most analyses on premixed turbulent combustion have been conducted for flames without any wall effects, and recent advancements in experimental diagnostics [2–4] and computational simulations [5–19] have enabled insightful analyses of FWI for turbulent premixed combustion. These analyses provided valuable insights into the flame structure and flow dynamics [2,8,12,20], wall heat flux [2–5,7,20–24], reactive scalar gradient [3,6,7,11,14–16,24–26], kinetic energy [9,13,27], turbulent scalar flux [10,27] and displacement speed [13,15,16,20,24,28] statistics close to the wall, and the resulting physical insights were utilised to develop high-fidelity models in the context of Flame Surface Density (FSD) [3,11,25,27,29] and Scalar Dissipation Rate (SDR) [6,7,11] methodologies. However, most of these analyses [3,5–12,25] were conducted for unsteady head-on quenching (HOQ) configurations under decaying turbulence and not under a statistically steady-state condition for FWI in TBLs. Bruneaux et al. [21,29] pioneered the computational analysis of FWI in a channel flow configuration but under constant density assumption for unsteady conditions. Alshaalan and Rutland [22,27], Gruber et al. [23], Ahmed et al. [15,16] and Jiang et al.

* Corresponding author.
E-mail address: markus.klein@unibw.de (M. Klein).

https://doi.org/10.1016/j.ijheatmasstransfer.2022.123230
0017-9310/© 2022 The Author(s). Published by Elsevier Ltd. This is an open access article under the CC BY-NC-ND license
(http://creativecommons.org/licenses/by-nc-nd/4.0/)

[19] analysed oblique wall flame-quenching (OWQ) of turbulent V-shaped premixed flames due to their interaction with isothermal inert walls within TBLs under statistically stationary state using three-dimensional Direct Numerical Simulations (DNS). Recent experiments [3,4] also analysed OWQ of turbulent V-shaped premixed flames in TBLs. These studies used the experimental data to assess the performances of the FSD and mean reaction rate models in the near-wall region [3]. Recently, Ahmed et al. [15] also assessed the Bray-Moss-Libby (BML) based modelling framework in the context of OWQ of V-shaped premixed flames in TBLs using DNS data. A semi-analytical derivation by Zhao et al. [20] demonstrated that the flame speed and wall heat flux are closely linked during flame quenching in a configuration where the flame impinges on an isothermal cold surface. However, the evolution of turbulent burning velocity with the progress of FWI in TBLs, and its dependence on wall heat flux are yet to be analysed in detail. The present analysis addresses this gap in the existing literature by deriving an integral form of the energy conservation equation. The validity of the integral energy equation derivation is verified using three-dimensional DNS data of a turbulent V-shaped premixed flame interacting with an isothermal inert wall. This integral energy equation is then utilised to establish the relation between turbulent burning velocity and wall heat flux and this relation in turn is utilised to illustrate the statistical behaviours of turbulent burning velocity and wall heat flux magnitude with the evolution of OWQ of V-shaped premixed flames in TBLs using DNS data.

2. Derivation of the energy integral

For small values of Mach number (i.e., $Ma \ll 1$), the pressure gradient terms in the energy conservation equation can be neglected [30] and under this assumption the energy conservation equation for a flat plate boundary layer takes the following form:

$$\frac{\partial(\rho h)}{\partial t} + \frac{\partial(\rho u h)}{\partial x} + \frac{\partial(\rho v h)}{\partial y} = \frac{\partial}{\partial x}(\lambda \frac{\partial T}{\partial x}) + \frac{\partial}{\partial y}(\lambda \frac{\partial T}{\partial y}) + \dot{\omega}_T. \quad (1)$$

Here, h is the specific sensible enthalpy, ρ is the gas density, T is the temperature, λ is the thermal conductivity, $\dot{\omega}_T$ is the heat release rate, and the flow direction is taken to align with x-direction, whereas the wall-normal direction is taken to be y-direction. The velocity components in x- and y-directions are given by u and v, respectively. On Reynolds averaging Eq. (1), the following expression for a statistically steady-state is obtained:

$$\frac{\partial(\bar{\rho}\tilde{u}\tilde{h})}{\partial x} + \frac{\partial(\bar{\rho}\tilde{v}\tilde{h})}{\partial y} = -\frac{\partial q_x}{\partial x} - \frac{\partial q_y}{\partial y} + \overline{\dot{\omega}_T}. \quad (2)$$

Here, $\bar{Q}$, $\tilde{Q} = \overline{\rho Q}/\bar{\rho}$ and $Q'' = Q - \tilde{Q}$ are the Reynolds average, Favre-average, and Favre fluctuation of a general quantity Q, respectively. In Eq. (2), $q_x = -\lambda(\partial\tilde{T}/\partial x) + \overline{\rho u'' h''}$ and $q_y = -\lambda(\partial\tilde{T}/\partial y) + \overline{\rho v'' h''}$ are mean heat fluxes in x- and y-directions, respectively. Within the thermal boundary layer $|-\partial q_y/\partial y| \gg |-\partial q_x/\partial x|$ and thus Eq. (2) can be simplified as:

$$\frac{\partial(\bar{\rho}\tilde{u}\tilde{h})}{\partial x} + \frac{\partial(\bar{\rho}\tilde{v}\tilde{h})}{\partial y} = -\frac{\partial q_y}{\partial y} + \overline{\dot{\omega}_T}. \quad (3)$$

Integrating Eq. (3) from the wall to the thermal boundary layer thickness δ_t (i.e., the wall normal distance where $\partial\tilde{T}/\partial y_{y=\delta_t} = 0$) yields the following expression using Leibnitz's theorem (see the Appendix for a detailed derivation):

$$\frac{d}{dx}\int_0^{\delta_t} \bar{\rho}\tilde{u}(\tilde{h} - \tilde{h}_\infty)dy + \frac{d\tilde{h}_\infty}{dx}\int_0^{\delta_t} \bar{\rho}\tilde{u}dy = \bar{q}_w + \int_0^{\delta_t} \overline{\dot{\omega}_T}dy, \quad (4)$$

where $\tilde{h}_{\delta_t} = \tilde{h}_\infty$ is the specific sensible enthalpy of the freestream and $\bar{q}_w = -\lambda(\partial\tilde{T}/\partial y)_{y=0} = (q_y)_{y=0}$ is the mean wall heat flux because $\overline{\rho v'' h''}$ is identically zero due to the impenetrability at the wall. At $y = \delta_t$, the heat flux $q_y = -\lambda(\partial\tilde{T}/\partial y) + \overline{\rho v'' h''}$ vanishes, which has been verified by interrogating the DNS data used for this analysis (not shown). At the edge of the thermal boundary layer $(\partial\tilde{T}/\partial y)$ vanishes by definition and at this location, there is no fluctuation of sensible enthalpy which leads to a vanishingly small value of $\overline{\rho v'' h''}$. The mean heat release rate can be expressed as $\overline{\dot{\omega}_T} = -\overline{\dot{\omega}_F}(h_{ad} - h_0)/(Y_{F_u} - Y_{F_b})$ where $\overline{\dot{\omega}_F}$, h_0, h_{ad}, Y_{F_u} and Y_{F_b} are the mean fuel reaction rate, specific enthalpy of reactants in the unburned gas, specific enthalpy of the fully burned products corresponding to the adiabatic flame temperature, fuel mass fractions in the unburned gas and fully burned products, respectively. The quantity $\overline{\dot{\omega}_c} = -\overline{\dot{\omega}_F}/(Y_{F_u} - Y_{F_b})$ is the mean reaction rate of reaction progress variable $c = (Y_{F_u} - Y_F)/(Y_{F_u} - Y_{F_b})$ which upon using in Eq. (4) yields:

$$\underbrace{\frac{d}{dx}\int_0^{\delta_t} \frac{\bar{\rho}\tilde{u}(\tilde{h} - \tilde{h}_\infty)}{\rho_0 u_{\tau,NR}(h_{ad} - h_0)}dy}_{T_1} + \underbrace{\frac{1}{(h_{ad} - h_0)}\frac{d\tilde{h}_\infty}{dx}\int_0^{\delta_t} \frac{\bar{\rho}\tilde{u}}{\rho_0 u_{\tau,NR}}dy}_{T_2} = \underbrace{\frac{\bar{q}_w}{\rho_0 u_{\tau,NR}(h_{ad} - h_0)}}_{T_3} + \underbrace{\frac{1}{\rho_0 u_{\tau,NR}}\int_0^{\delta_t} \overline{\dot{\omega}_c}dy}_{T_4}. \quad (5)$$

In Eq. (5) ρ_0 is the unburned gas density, $\bar{q}_w$ is the mean wall heat flux, $u_{\tau,NR} = \sqrt{(|\tau_{w,NR}|/\rho_0)}$ is the friction velocity for the corresponding non-reacting flow with $\tau_{w,NR} = \mu(\partial u/\partial y)_{y=0}$ being the corresponding wall shear stress. Eq. (5) will henceforth be referred to as the energy integral equation. The term T_1 accounts for advection effects, whereas T_2 addresses the effects of the freestream temperature variation. The term T_3 arises due to wall heat flux, whereas T_4 arises due to a chemical reaction within the TBL. Although Eq. (5) is derived for TBL, the energy integral equation can be applied to laminar boundary layers in the case of premixed FWI when the Favre-averaged and Reynolds-averaged values are replaced by the corresponding instantaneous quantities. It is worth noting that T_3 can be expressed as:

$$T_3 = \frac{\bar{q}_w}{\rho_0 u_{\tau,NR}(h_{ad} - h_0)} = \frac{-H_{t,x}}{\rho_0 u_{\tau,NR} C_{P0}} = -St_\tau = \frac{-Nu_x}{Re_\tau Pr}, \quad (6)$$

where $H_{t,x} = C_{P0}|q_w|/(h_{ad} - h_0)$ is the local heat transfer coefficient, St_τ is the Stanton number, $Re_\tau = \rho_0 u_{\tau,NR}\Delta_h/\mu_0$ is the friction velocity based Reynolds number and $Nu_x = H_{t,x}\Delta_h/\lambda_0$ is the local Nusselt number with C_{P0}, μ_0 and λ_0 being the unburned gas specific heat capacity, unburned gas viscosity, and unburned gas thermal conductivity, respectively and Δ_h is a reference length scale which is taken to be the channel half height for the current analysis. Integrating Eq. (5) between $x = L_1$ and $x = L_2$ yields: $\int_{L_1}^{L_2}(T_1 + T_2)L_W dx = \int_{L_1}^{L_2}(T_3 + T_4)L_W dx$ with L_W being the width of the flat plate. These relations lead to:

$$T_{1L} + T_{2L} = \frac{-Nu_L}{Re_\tau Pr} + \frac{A_{proj}S_T}{A_{seg}u_{\tau,NR}}, \quad (7)$$

where $T_{1L} = (L_2 - L_1)^{-1}\int_{L_1}^{L_2} T_1 dx$, $T_{2L} = (L_2 - L_1)^{-1}\int_{L_1}^{L_2} T_2 dx$, A_{proj} is the projected flame surface area, $A_{seg} = (L_2 - L_1)L_W$ is the area of the segment, $Nu_L = (L_2 - L_1)^{-1}\int_{L_1}^{L_2} Nu_x dx$ is the mean Nusselt number, and $S_T = (\rho_0 A_{proj})^{-1}\int_{L_1}^{L_2}\int_0^{\delta_t} \overline{\dot{\omega}_c} L_W dx dy$ is the turbulent burning velocity [31], subject to the assumption that the flame is contained within the thermal boundary layer, which suggests that $\overline{\dot{\omega}_c}$ vanishes at $y = \delta_t$. Eq. (7) indicates that Nu_L and S_T are not independent of each other in the case of premixed FWI in TBLs, and therefore upon evaluating one of these quantities the other can be found, provided the variations of $\tilde{u}$ and $\tilde{h}$ with the wall normal direction are obtained.

3. DNS database

The newly derived energy integral equation for premixed FWI in flat plate TBL has been validated using three-dimensional DNS of a turbulent V-shaped flame interacting with an isothermal inert wall in a channel flow configuration. A detailed discussion on the numerical implementation of the DNS database including the validation of the non-reacting channel flow solution can be found elsewhere [15,16]. Only a brief discussion is provided here. The simulation has been carried out using a uniform Cartesian grid-based compressible DNS code SENGA+ [6–12,14–16,24,25,28] where all the spatial derivatives are evaluated using a high-order finite-difference scheme (10th order central difference scheme for the internal grid points but the order of accuracy gradually reduces to 2nd order at the non-periodic boundaries) and time advancement has been carried out using a low storage 3rd order Runge–Kutta scheme. A non-reacting turbulent plane channel flow driven by a constant streamwise pressure gradient (i.e. $-\partial p/\partial x = \rho u_{\tau,NR}^2/\Delta_h$, where p is the pressure) has been conducted in order to obtain the initial condition for the reacting flow simulation and for inlet boundary condition specifications. The bulk Reynolds number for this simulation is taken to be $Re_b = 2\rho_0 u_b \Delta_h/\mu_0 = 3285$, where $u_b = (1/2\Delta_h)\int_0^{2\Delta_h} u dy$ is the bulk mean velocity, which corresponds to a friction velocity based Reynolds number $Re_\tau = \rho_0 u_{\tau,NR}\Delta_h/\mu_0 = 110$. This simulation ensures that the maximum value of $y^+ = \rho_0 u_{\tau,NR} y/\mu_0$ for the grid points adjacent to the wall remains approximately 0.6 following Moser et al. [32]. This grid spacing ensures that the domain of $L_x \times L_y \times L_z = 10.69\Delta_h \times 2\Delta_h \times 4\Delta_h$ is discretised by $1920 \times 360 \times 720$, which accommodates 8 grid points within the thermal flame thickness $\delta_{th} = (T_{ad} - T_0)/\max|\nabla T|_L$ (where T_0, T_{ad} and T are the unburned gas temperature, adiabatic flame temperature and instantaneous temperature, respectively). Here, $S_L/u_{\tau,NR}$ is taken to be 0.7 with S_L being the unstretched laminar burning velocity.

The chemical processes are taken to be representative of stoichiometric methane-air premixed flames preheated to $T_0 = 730$ K following previous analyses [15,16,22,23,27], yielding a heat release parameter $\alpha_H = (T_{ad} - T_0)/T_0 = 2.3$. A single step chemical reaction (i.e., 1.0 unit mass of fuel+ s unit mass of Oxygen $= (1+s)$ unit of products with $s = 4.0$) is considered for the sake of computational economy. It is worthwhile to note that previous analyses [11,12] demonstrated that wall heat flux, quenching distance and near-wall vorticity dynamics obtained from detailed chemistry DNS for hydrocarbon-air premixed FWI are adequately captured by single-step chemistry and the FWI models developed by single step chemistry remain valid for detailed chemistry DNS. Interested readers are referred to Refs. [9,11,15,16] for further information in this regard. Moreover, several previous analyses [5–12,14–16,20–22,24,25,27,29,33] provided important insights into premixed FWI using simple chemistry and the same approach has been adopted here. Note that the derivation of Eqs. (4)–(7) does not depend on the choice of chemical mechanism, and thus the chemical representation of this DNS data does not alter the conclusions drawn in this paper. Standard values are chosen for the Zel'dovich number (i.e. $\beta_Z = T_{ac}(T_{ad} - T_0)/T_{ad}^2 = 6.0$ where T_{ac} is the activation temperature), Prandtl number (i.e. $Pr = 0.7$), ratio of specific heats (i.e. $\gamma = 1.4$) and Lewis numbers for all species are considered to be unity. The pressure gradient terms in the energy conservation equation in both boundary layers and channel flows can be dropped when the Eckert number is small (i.e. $Ec \ll 1.0$) [30]. For the current channel flow configuration, the Eckert number can be defined as: $Ec = u_{\tau,NR}^2/(h_{ad} - h_0) = (\gamma - 1)Ma^2/\alpha_H$ where $Ma = u_{\tau,NR}/a_0$ is the Mach number with a_0 being the acoustic speed in the unburned gas. For the present analysis, $Ma = 3 \times 10^{-3}$ which suggests an Eckert number of $Ec = 1.56 \times 10^{-6}$ for the case considered here. This justifies the usage of the form of the energy conservation equation given by Eq. (1). For the reacting flow simulation, the flame holder is placed within the fully-developed channel flow at a location such that the centre of the flame holder is $0.83\Delta_h$ from the inlet and $0.5\Delta_h$ (i.e. corresponds to $y^+ = 55$) from the bottom wall. The flame holder was intentionally kept closer to the bottom wall than to the top wall because it ensures FWI for the bottom wall takes place within the domain, whereas the top branch of the V-flame does not interact within the computational domain. The location of the flame holder centre is chosen in such a manner that the flame holder does not influence the viscous sublayer. The species mass fractions, velocity components and temperature are specified using a Gaussian function following Dunstan et al. [34] and further details are provided elsewhere [15,16]. The radius of the flame holder is taken to be $0.5\delta_{th}$. The turbulent inflow with specified density and velocity components from non-reacting flow simulations, and partially non-reflecting outflow boundaries are specified in the x-direction. Isothermal inert walls with the same temperature as the unburned gas temperature (i.e. $T_{y=0} = T_{y=2\Delta_h} = T_0$) are considered for y-boundaries. This implies that the fluid-dynamic boundary layer exists throughout the simulation domain in this configuration, whereas the thermal boundary layer forms only in the region of the simulation where the FWI takes place. The boundaries in the z-direction are considered to be periodic. All the boundaries are specified using an improved version of the Navier–Stokes Characteristic Boundary condition [35]. The simulation has been continued for 3.0 flow through times (i.e., $3.0L_x/u_b$), and statistics have been extracted after one flow through time once the initial transience has decayed. The Reynolds/Favre averaged quantities are evaluated by time-averaging and subsequently by spatial averaging in the statistically homogeneous z-direction.

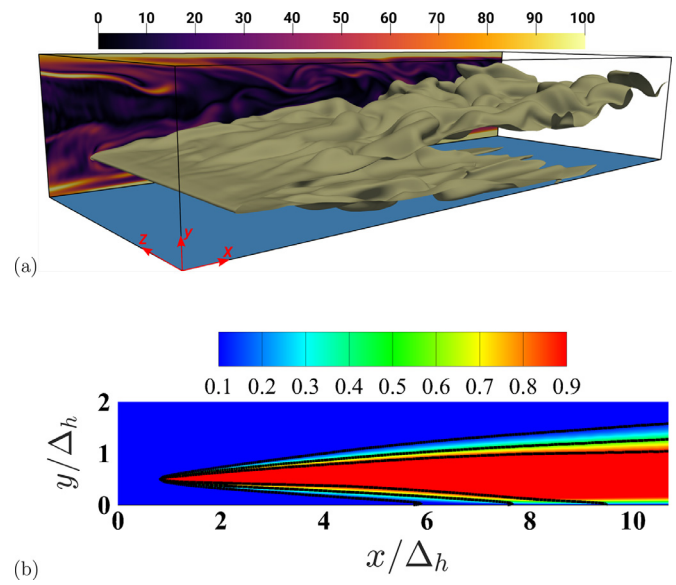

Fig. 1. (a) Schematic diagram of the simulation domain along with the $c = 0.5$ isosurface with the normalised vorticity magnitude ($\sqrt{(\omega_i\omega_i)} \times \Delta_h/u_{\tau,NR}$ in the $z/\Delta_h = 4.0$ plane, (b) distribution of $\tilde{\theta} = (\tilde{T} - T_0)/(T_{ad} - T_0)$ with the contour lines of $\tilde{c} = 0.1$, 0.5 and 0.9 superimposed.

4. Results and discussions

The $c = 0.5$ isosurface with the normalised vorticity magnitude $\sqrt{(\omega_i\omega_i)} \times \Delta_h/u_{\tau,NR}$ (where ω_i is the ith component of vorticity) in the central midplane is provided in Fig. 1a, which shows the visual representations of wall ejections, flame wrinkling and quench-

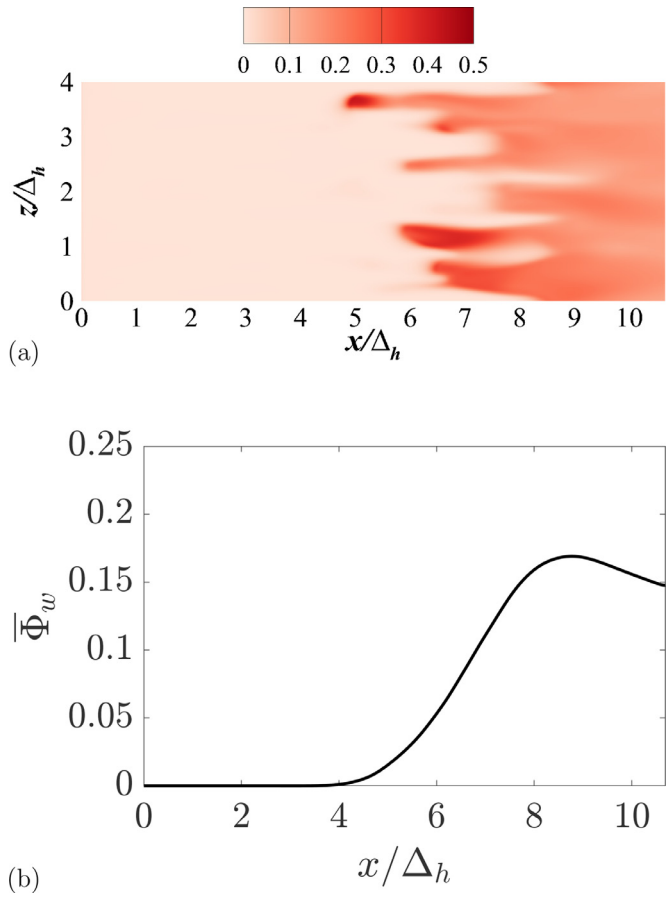

Fig. 2. (a) Instantaneous distribution of normalised wall heat flux magnitude $\Phi_w = |q_w|/[\rho_0 S_L(h_{ad} - h_0)]$ on the bottom wall, (b) variation of $\overline{\Phi}_w$ with x/Δ_h.

ing near the bottom wall. The distribution of the Favre averaged values of the non-dimensional temperature $\tilde{\theta} = (\tilde{T} - T_0)/(T_{ad} - T_0)$ are shown in Fig. 1b with the contour lines of Favre averaged values of reaction progress variable $\tilde{c} = 0.1, 0.3, 0.5, 0.7$ and 0.9 superimposed. It is worth noting that in the configuration analysed here the fluid-dynamic boundary layer exists throughout the domain, whereas the thermal boundary layer starts only when the flame-wall interaction takes place because the walls are kept at the same temperature as that of the unburned gas. A major part of the channel in the region of the flame-wall interaction is occupied by the fully burned gas where there is no variation of temperature. It is evident from Fig. 1a and b that the flame surface interacts with the bottom wall within the simulation domain, and the validity of the energy integral equation (i.e., Eq. (5)) is assessed for the TBL on the bottom wall over which the thermal boundary layer develops in this configuration.

Fig. 1 a shows that the flame surface starts to interact with the bottom wall at around $x/\Delta_h = 5.0$ and completely quenches at around $x/\Delta_h = 10.5$ in this configuration, which can be substantiated from the instantaneous distribution of normalised wall heat flux magnitude $\Phi_w = |q_w|/[\rho_0 S_L(h_{ad} - h_0)]$ on the bottom wall, shown in Fig. 2a. It can be seen from Fig. 2a that the non-zero values of Φ_w are predominantly obtained for $x/\Delta_h > 5.0$. Moreover, the distribution of $\tilde{\theta}$ in Fig. 1b shows that the flame surface starts to interact with the inert isothermal bottom wall at $x/\Delta_h = 4.0$ and the flame completely quenches at around $x/\Delta_h = 10$ in a mean sense. This can be confirmed from Fig. 2b where the variation of mean normalised wall heat flux magnitude $\overline{\Phi}_w = |\bar{q}_w|/[\rho_0 S_L(h_{ad} - h_0)] = St_\tau(u_{\tau,NR} S_L)$ with x/Δ_h is shown. It can be seen from Fig. 2a and b that the FWI is intermittent for $5 \le x/\Delta_h \le 6$ and the flame is fully quenched by $x/\Delta_h = 10$ and thus including $10 \le x/\Delta_h \le 10.69$ does not provide any extra insights. Furthermore, the energy integral equation is valid only where the boundary layer assumption is valid so examining where the boundary layer assumption [36] is not valid does not add much value to the discussion, and thus the terms of Eqs. (5) and (7) will be analysed for $10.0 \ge x/\Delta_h \ge 6.0$. The locations $x/\Delta_h = 6.0$ and 10 correspond to a disctance of $5.17\Delta_h$ and $9.17\Delta_h$ from the flame holder in the stremwise direction.

The distributions of $\tilde{u}/u_{\tau,NR}$ and $\tilde{\theta}$ with y/Δ_h are shown in Fig. 3a and b, respectively for $x/\Delta_h = 6.0, 7.0, 8.0, 9.0$ and 10.0 and the corresponding values of $\partial\tilde{u}/\partial y \times \Delta_h/u_{\tau,NR}$ and $\partial\tilde{\theta}/\partial y \times \Delta_h$ are shown in Fig. 3c and d, respectively. The wall normal distance to the location where $|\partial\tilde{\theta}/\partial y| \times \Delta_h \le 10^{-3}$ is taken to be the thermal boundary layer thickness δ_t, which is shown by the vertical lines in Fig. 3. It can be seen from Fig. 3 that the velocity gradient $\partial\tilde{u}/\partial y$ also almost vanishes at the edge of the thermal boundary layer (i.e. $y = \delta_t$). It can be seen from Fig. 2a, b that the thermal boundary layer starts at around $x/\Delta_h \approx 5$ and the resulting thermal boundary layer thickness remains smaller than the channel half-height Δ_h (i.e. $\delta_t/\Delta_h < 1.0$, see Fig. 3) within the simulation domain. Fig. 3 further shows that $\partial\tilde{u}/\partial y$ remains small at the edge of the thermal boundary layer for $6 \le x/\Delta_h \le 10$ and $\partial\tilde{\theta}/\partial y$ disappears at the edge of the thermal boundary layer, by definition. These combinations resemble the classical picture of the thermal boundary layer in unconfined boundary layer flows. It is also worth noting from Fig. 3 that $\tilde{\theta}$ assumes a value of unity at the edge of the thermal boundary layer (i.e. $y = \delta_t$), which suggests that the mean reaction rate of reaction progress variable $\bar{\dot{\omega}}_c$ also vanishes at the edge of the thermal boundary layer. This can be seen from the variations of $\bar{\dot{\omega}}_c \times \Delta_h/\rho_0 u_{\tau,NR}$ with y/Δ_h for the bottom wall in Fig. 4, which shows that the mean reaction rate vanishes in the vicinity of the wall because of flame quenching as a result of wall heat loss and low wall temperature. Fig. 4 also demonstrates that $\bar{\dot{\omega}}_c \times \Delta_h/\rho_0 u_{\tau,NR}$ vanishes at the edge of the thermal boundary layer because of the complete consumption of fuel in the burned gas.

The variations of $T_1, T_2, (-T_3), (-T_4)$ and $(T_1 + T_2) - (T_3 + T_4)$ at $x/\Delta_h = 6.0, 7.0, 8.0, 9.0$ and 10.0 are shown in Fig. 5. It can be seen from Fig. 5 that T_4 remains positive but its magnitude decreases with increasing x/Δ_h with the progress of flame quenching. The term T_3 (alternatively $-T_3$) assumes negative (alternatively positive) values and its magnitude increases with increasing x/Δ_h due to the increase in wall heat flux magnitude as a result of flame quenching. It can further be seen from Fig. 5 that T_2 remains negligible in comparison to T_1, T_3 and T_4. As the edge of the thermal boundary layer in this configuration is always in the burned gas where $\tilde{h}_{\delta_t} = \tilde{h}_\infty = h_{ad}$, the term $d\tilde{h}_\infty/dx$ vanishes at all the locations. This gives rise to a vanishingly small value of T_2 in this configuration. However, this may not be valid for other configurations and thus this term is retained for the sake of completeness. However, the contribution of T_{2L} in Eq. (7) will henceforth be ignored in this analysis. The net contribution of $(T_1 + T_2) - (T_3 + T_4)$ assumes vanishingly small values at $x/\Delta_h = 6.0, 7.0, 8.0, 9.0$ and 10.0, as expected under statistically stationary state according to Eq. (5). The variations of T_{1L}, $(-Nu_L/[Re_\tau Pr])$ and $A_{proj} S_T/[A_{seg} u_{\tau,NR}]$ for four different streamwise segments between $x/\Delta_h = 6.0$ and $x/\Delta_h = 10.0$ along with the corresponding variations for $10.0 \ge x/\Delta_h \ge 6.0$ are shown in Fig. 6 where the projected flame surface area A_{proj} is estimated as $L_W(L_2 - L_1)/cos\phi$ with $\phi = 3.07^o$ being the angle of the $\tilde{c} = 0.94$ contour with the x-axis. The value of $\tilde{c}$ is chosen such that its iso-contour exists up to $x/\Delta_h \ge 10.0$. The iso-contours of smaller values of $\tilde{c}$ vanish before $x/\Delta_h \le 10.0$. However, the iso-contours of smaller values of $\tilde{c}$ make an angle in the range of $\phi = 4^\circ$ to 5° with the x-axis. Therefore, there is a negligible variation in the estimation of projected flame surface area,

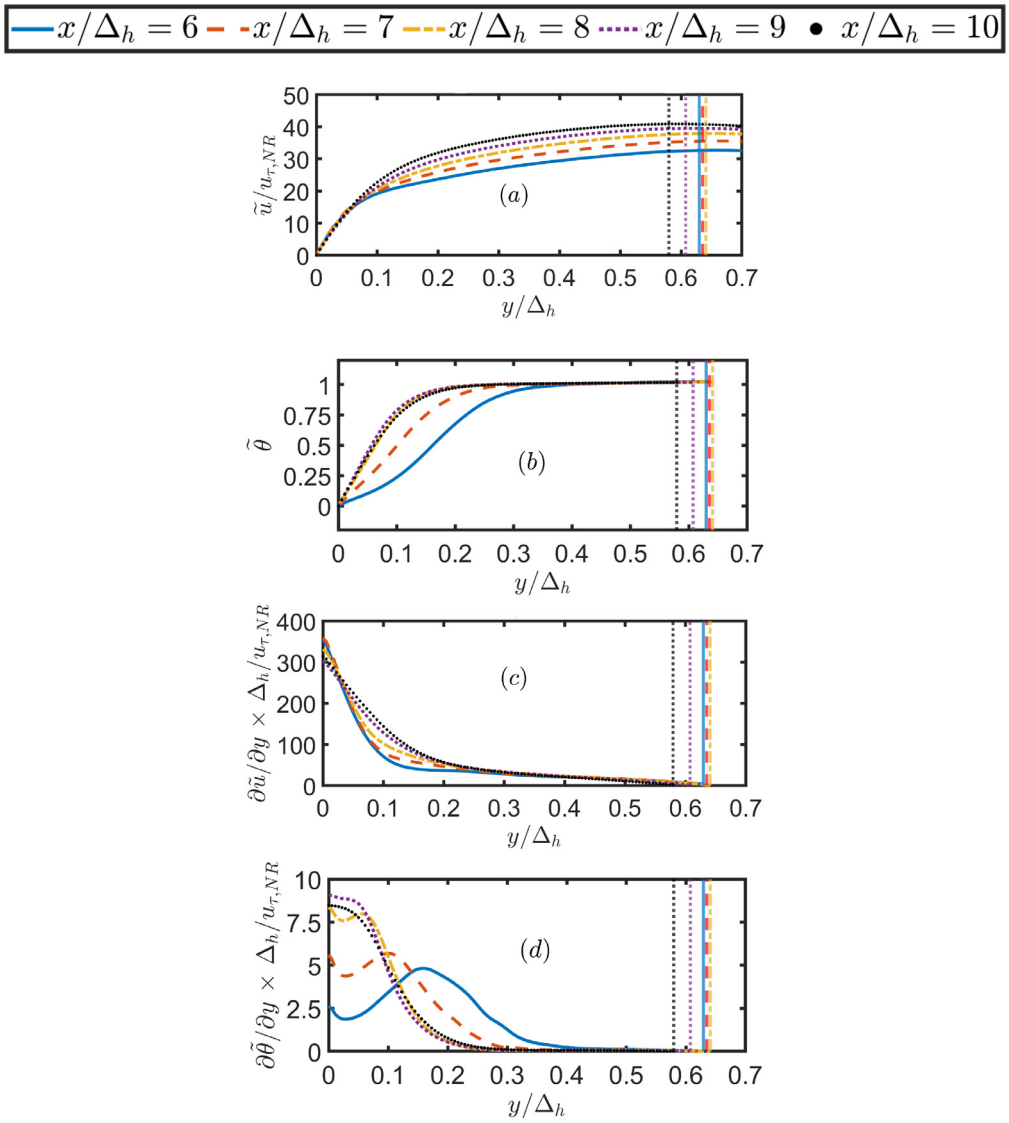

Fig. 3. Distributions of (a) $\tilde{u}/u_{\tau,NR}$, (b) $\tilde{\theta}$, (c) $\partial\tilde{u}/\partial y \times \Delta_h/u_{\tau,NR}$ and (d) $\partial\tilde{\theta}/\partial y \times \Delta_h$ with y/Δ_h for $x/\Delta_h = 6.0, 7.0, 8.0, 9.0$ and 10.0. Vertical lines represents the thermal boundary layer thickness δ_t. The flame holder location corresponds to $x/\Delta_h = 0.83$.

A_{proj} with different choices of $\tilde{c}$ due to the marginal variation in the $cos\phi$ values. It can be seen from Fig. 6 that the behaviours of T_{1L}, $(-(Nu_L)/[Re_\tau Pr])$ and $A_{proj}S_T/[A_{seg}u_{\tau,NR}]$ with x/Δ_h are qualitatively similar to those of T_1, T_3 and T_4 shown in Fig. 5.

It can further be seen from Fig. 6 that the net contribution of $-Nu_L/[Re_\tau Pr] + A_{proj}S_T/[A_{seg}u_{\tau,NR}]$ remains almost equal to T_{1L} because of the negligible value of T_{2L}. In physical terms, a part of the heat release due to combustion is lost through the wall due to $-Nu_L/[Re_\tau Pr]$ and the remaining part is accounted by the advection effects represented by T_{1L}. The results reported in Fig. 6 suggest that the Nusselt number and turbulent burning velocity are closely related in the case of FWI in TBLs. Therefore, evaluations of $\tilde{u}$ and $\tilde{\theta}$ distributions and the knowledge of the mean Nusselt number enables the estimation of the turbulent burning velocity in TBLs. Conversely, the knowledge of turbulent burning velocity, $\tilde{u}$ and $\tilde{\theta}$ distributions in TBLs enables the estimation of the Nusselt number. Based on this, it is worthwhile to consider if S_T can be estimated using one of the existing closures of turbulent premixed combustion modelling. Sellmann et al. [25] proposed that the mean reaction rate $\bar{\dot{\omega}}_c$ in the case of HOQ can be modelled as $\bar{\dot{\omega}}_c = I_0\rho_0 S_L \Sigma_{gen}$ where $I_0 = 0.5[erf(y/\delta_z - Pe_Q) + 1]$ accounts for near-wall damping of reaction rate effects due to flame quenching, where $\delta_z = \alpha_{T_0}/S_L$ is the Zel'dovich flame thickness, $Pe_Q = \delta_Q/\delta_z$ is the wall Peclet number for the laminar HOQ configuration (=2.19 for the present thermochemistry [15]) with α_{T_0} and δ_Q being the thermal diffusivity in the unburned gas and δ_Q is the quenching distance for HOQ of laminar premixed flames. The predictions of $I_0\rho_0 S_L \Sigma_{gen}$ are compared to $\bar{\dot{\omega}}_c$ extracted from DNS data in Fig. 4, which reveals that $I_0\rho_0 S_L \Sigma_{gen}$ captures the qualitative behaviour of $\bar{\dot{\omega}}_c$ both in the vicinity as well as away from the wall at all locations considered here. However, there is an underprediction in the outer layer of the TBL at $x/\Delta_h = 6.0$ and the FSD model overpredicts the mean reaction rate $\bar{\dot{\omega}}_c$ in the near-wall region for $x/\Delta_h \geq 7.0$. The discrepancy between the DNS data and model prediction originates due to the limitation of the model for the stretch factor I_0 and the local discrepancies between the mean reaction rate and the FSD-based reaction rate closure in the outer layer exist as well for other flows without boundary layers [25,37]. Alternative expressions of I_0 for FWI were previously proposed for FWI [21,27], but it was shown by Sellmann et al. [25] and Ahmed et al. [15] that $I_0 = 0.5[erf(y/\delta_z - Pe_Q) + 1]$ provides more accurate prediction of $\bar{\dot{\omega}}_c$ in comparison to other alternatives [21,27]. It is also

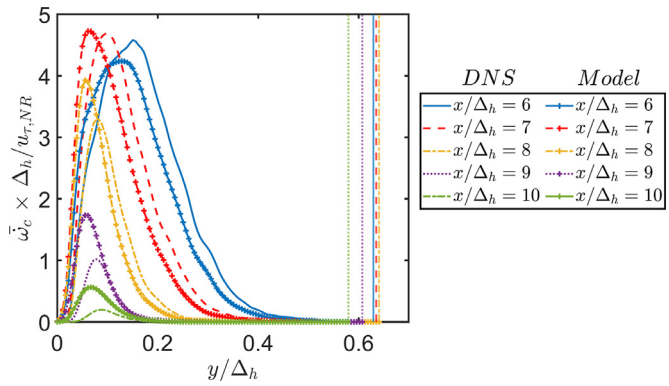

Fig. 4. Variations of $\bar{\dot{\omega}}_c \times \Delta_h/\rho_0 u_{\tau,NR}$ (lines) with y/Δ_h for the bottom wall along with the predictions of $I_0\rho_0 S_L \Sigma_{gen} \times \Delta_h/\rho_0 u_{\tau,NR}$ (lines with symbols) where $I_0 = 0.5[erf(y/\delta_z - Pe_Q) + 1]$ for $x/\Delta_h = 6.0, 7.0, 8.0, 9.0$ and 10.0. Vertical lines represents the thickness of the thermal boundary layer thickness δ_t. The flame holder location corresponds to $x/\Delta_h = 0.83$.

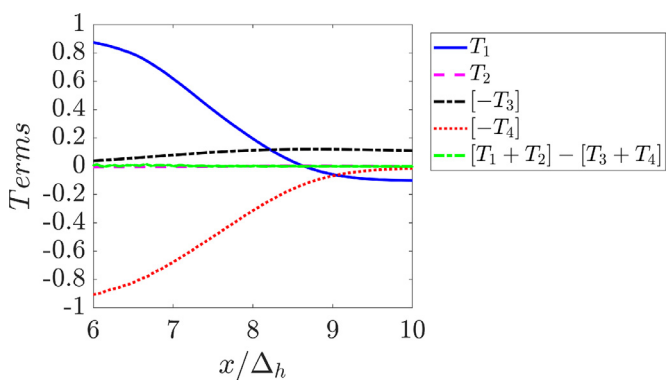

Fig. 5. Variations of $T_1, T_2, -T_3, -T_4$ and $(T_1 + T_2) - (T_3 + T_4)$ (see Eq. (5)) at $x/\Delta_h = 6.0, 7.0, 8.0, 9.0$ and 10.0. The flame holder location corresponds to $x/\Delta_h = 0.83$.

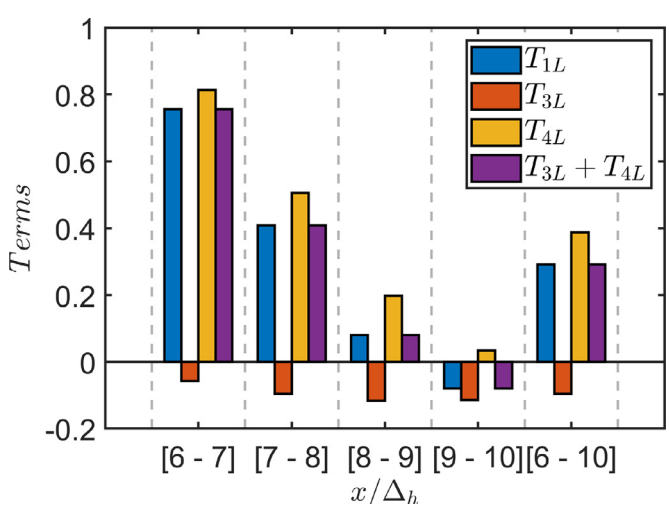

Fig. 6. Variations of $T_{1L}, T_{3L} = -(Nu_L)/[Re_\tau Pr]$, $T_{4L} = A_{proj}S_T/[A_{seg}u_{\tau,NR}]$ and $T_{3L} + T_{4L}$ (see Eq. (7)) for $7.0 \geq x/\Delta_h \geq 6.0$, $8.0 \geq x/\Delta_h \geq 7.0$, $9.0 \geq x/\Delta_h \geq 8.0$, $10.0 \geq x/\Delta_h \geq 9.0$ along with the corresponding variations for $10.0 \geq x/\Delta_h \geq 6.0$. The flame holder location corresponds to $x/\Delta_h = 0.83$.

worth noting that $I_0 = 0.5[erf(y/\delta_z - Pe_Q) + 1]$ for FWI was proposed for HOQ and here it is used for oblique flame quenching and thus there is scope to improve the $\bar{\dot{\omega}}_c$ predictions by modifying I_0 for the oblique quenching.

The predictions of $S_T^{model} = (\rho_0 A_{proj})^{-1} \int_{L_1}^{L_2}\int_0^{\delta_t} I_0\rho_0 S_L \Sigma_{gen} L_W dxdy$ are compared to $S_T = (\rho_0 A_{proj})^{-1} \int_{L_1}^{L_2}\int_0^{\delta_t}$

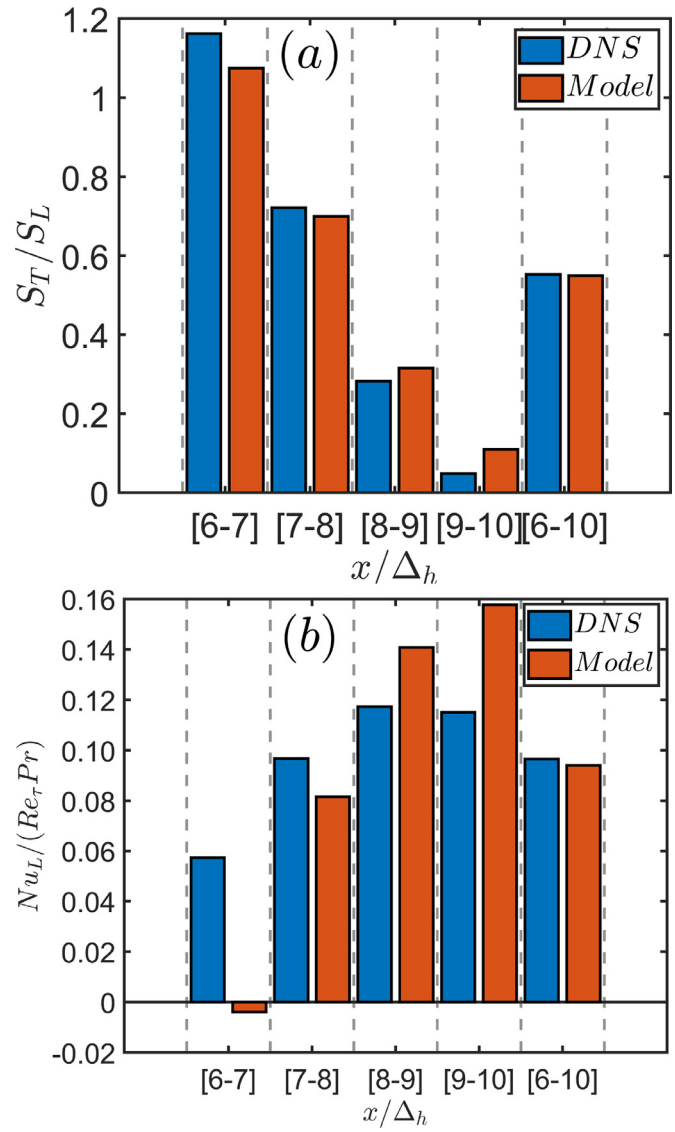

Fig. 7. (a) Predictions of S_T^{model}/S_L along with S_T/S_L extracted from DNS data for $7.0 \geq x/\Delta_h \geq 6.0$, $8.0 \geq x/\Delta_h \geq 7.0$, $9.0 \geq x/\Delta_h \geq 8.0$, $10.0 \geq x/\Delta_h \geq 9.0$ and also for $10.0 \geq x/\Delta_h \geq 6.0$, (b) predictions of $Nu_L/[Re_\tau Pr]$ by using S_T^{model} in Eq. (7) compared to $Nu_L/[Re_\tau Pr]$ extracted from DNS data. The flame holder location corresponds to $x/\Delta_h = 0.83$.

$\bar{\dot{\omega}}_c L_W dxdy$ extracted from DNS data for four streamwise segments between $x/\Delta_h = 6.0$ and $x/\Delta_h = 10.0$ and also for $10.0 \geq x/\Delta_h \geq 6.0$ in Fig. 7a. Fig. 7a indicates that S_T^{model}/S_L underpredicts S_T/S_L obtained from DNS data for $6.0 \leq x/\Delta_h \leq 7.0$ and S_T^{model} overpredicts S_T for $8.0 \geq x/\Delta_h \geq 7.0$, $9.0 \geq x/\Delta_h \geq 8.0$, and $10.0 \geq x/\Delta_h \geq 9.0$. This behaviour originates due to the discrepancies between $I_0\rho_0 S_L \Sigma_{gen}$ and $\bar{\dot{\omega}}_c$, as can be noticed from Fig. 4. However, S_T^{model}/S_L predictions are found to be in excellent agreement with S_T/S_L obtained from DNS data when $10.0 \geq x/\Delta_h \geq 6.0$ is considered, as local overpredictions and underpredictions cancel each other.

In principle, an accurate estimation of S_T by S_T^{model} enables one to estimate Nu_L using Eq. (7). The Nu_L values estimated using S_T^{model} in Eq. (7) are compared to the corresponding value extracted from DNS data in Fig. 7b. Fig. 7b shows that Nu_L estimated using S_T^{model} does not agree with the corresponding value obtained from DNS data for $6.0 \leq x/\Delta_h \leq 7.0$ and in fact an incorrect sign of Nu_L is obtained. This discrepancy originates due to the underprediction

of S_T by S_T^{model} at $6.0 \le x/\Delta_h \le 7.0$ (see Fig. 7a). Moreover, Nu_L estimated using S_T^{model} does not agree with the corresponding value extracted from DNS data for $8.0 \ge x/\Delta_h \ge 7.0$, $9.0 \ge x/\Delta_h \ge 8.0$, and $10.0 \ge x/\Delta_h \ge 9.0$, and this is consistent with the overprediction of S_T by S_T^{model} at these locations. However, in accordance with Fig. 7a, Nu_L predictions using S_T^{model} in Eq. (7) are found to be in excellent agreement with Nu_L obtained from DNS data for $10.0 \ge x/\Delta_h \ge 6.0$. Despite this agreement, the findings from Fig. 7 suggest that it might be preferable to extract turbulent burning velocity based on the measurements of mean values of velocity, temperature and wall heat flux instead of predicting the mean Nusselt number based on model expressions of turbulent burning velocity. The measurement of wall heat flux in reacting gas flows is well-established in the literature [38–40] and this can be utilised in conjunction with the energy integral equation to estimate the turbulent burning velocity within turbulent boundary layers during FWI.

5. Conclusions

A newly derived integral form of the energy conservation equation has been derived for statistically steady premixed FWI within TBLs under low Mach number conditions. The validity of this equation is assessed at different locations of TBL in the case of statistically stationary oblique quenching of a turbulent premixed V-shaped flame in a channel due to its interaction with an inert isothermal wall based on three-dimensional DNS data. It has been found that the wall heat flux and the heat release rate remain the leading order contributors to the integral form of the energy conservation equation and their net contribution is balanced by the contribution arising from the advection process. The magnitudes of the wall heat flux increase and the contribution of heat release rate integral in the wall normal direction decrease with increasing distance from the leading edge of the thermal boundary layer as a result of flame quenching. The integral form of the energy conservation equation has been utilised to demonstrate that the Nusselt number (or Stanton number) for wall heat transfer is closely related to the turbulent burning velocity within TBLs. A methodology using the FSD based reaction rate closure revised to account for near-wall behaviour [15,25] has been shown to reasonably capture the behaviour of the turbulent burning velocity within the TBL only when a sufficiently large span of distance is considered. Thus, the modelling limitations in the mean reaction rate closure may give rise to significant inaccuracies in the estimation of the mean Nusselt number. This suggests that the measurements of mean velocity, temperature and wall heat flux can be utilised to estimate the turbulent burning velocity within TBLs. Although the validity of the current analysis does not depend on the choice of the chemical mechanism, the analysis conducted in this paper needs to be repeated in the presence of detailed chemistry and transport for further validation. Moreover, the usefulness of the newly derived energy integral equation needs to be explored further for other FWI configurations including unconfined spatially evolving turbulent boundary layers as well as flows with higher values of Re_τ. Some of these issues will form the basis of the future investigations.

Declaration of Competing Interest

The authors declare that they have no known competing financial interests or personal relationships that could have appeared to influence the work reported in this paper.

CRediT authorship contribution statement

Sanjeev Kr. Ghai: Formal analysis, Investigation, Visualization, Writing – review & editing. **Umair Ahmed:** Supervision, Visualization, Writing – review & editing. **Markus Klein:** Funding acquisition, Writing – review & editing. **Nilanjan Chakraborty:** Conceptualization, Formal analysis, Investigation, Supervision, Writing – original draft, Writing – review & editing.

Data Availability

Data will be made available on request.

Acknowledgements

The authors are grateful for the financial and computational support from the Engineering and Physical Sciences Research Council (Grant: EP/V003534/1, EP/R029369/1), CIRRUS, SuperMUC-NG (Grant: pn69ga, pn34xu), and ROCKET HPC facility.

Appendix A

Integrating Eq. (3) from the wall to the edge of the thermal boundary layer $y = \delta_t$ gives rise to:

$$\int_0^{\delta_t} \frac{\partial(\bar{\rho}\tilde{u}\tilde{h})}{\partial x} dy + \int_0^{\delta_t} \frac{\partial(\bar{\rho}\tilde{v}\tilde{h})}{\partial y} dy = -\int_0^{\delta_t} \frac{\partial q_y}{\partial y} dy + \int_0^{\delta_t} \overline{\dot{\omega}_T} dy \tag{A.1}$$

Eq. (A.1) leads to:

$$\int_0^{\delta_t} \frac{\partial(\bar{\rho}\tilde{u}\tilde{h})}{\partial x} dy + \bar{\rho}_{\delta_t}\tilde{v}_{\delta_t}\tilde{h}_{\delta_t} = \bar{q}_w - (\overline{\rho v'' h''})_{\delta_t} + \int_0^{\delta_t} \overline{\dot{\omega}_T} dy \tag{A.2}$$

The contribution of $(\overline{\rho v'' h''})_{\delta_t}$ is expected to be negligible at the edge of the thermal boundary layer, and thus it can be neglected (and it is confirmed using DNS data in this analysis but not shown for the sake of brevity). Using the Leibnitz theorem one can write:

$$\frac{d}{dx}\int_0^{\delta_t} (\bar{\rho}\tilde{u}\tilde{h}) dy = \int_0^{\delta_t} \frac{\partial(\bar{\rho}\tilde{u}\tilde{h})}{\partial x} dy + \bar{\rho}_{\delta_t}\tilde{u}_{\delta_t}\tilde{h}_{\delta_t}\frac{d\delta_t}{dx} \tag{A.3}$$

$$\frac{d}{dx}\int_0^{\delta_t} (\bar{\rho}\tilde{u}\tilde{h}_\infty) dy = \int_0^{\delta_t} \frac{\partial(\bar{\rho}\tilde{u}\tilde{h}_\infty)}{\partial x} dy + \bar{\rho}_{\delta_t}\tilde{u}_{\delta_t}\tilde{h}_\infty\frac{d\delta_t}{dx} \tag{A.4}$$

Using Eq. (A.4) and $\tilde{h}_{\delta_t} = \tilde{h}_\infty$, the last term on the right-hand side of Eq. (A.3) can be eliminated in the following manner:

$$\frac{d}{dx}\int_0^{\delta_t} (\bar{\rho}\tilde{u}\tilde{h}) dy = \int_0^{\delta_t} \frac{\partial(\bar{\rho}\tilde{u}\tilde{h})}{\partial x} dy + \frac{d}{dx}\int_0^{\delta_t} (\bar{\rho}\tilde{u}\tilde{h}_\infty) dy - \int_0^{\delta_t} \frac{\partial(\bar{\rho}\tilde{u}\tilde{h}_\infty)}{\partial x} dy \tag{A.5}$$

This leads to:

$$\frac{d}{dx}\int_0^{\delta_t} \bar{\rho}\tilde{u}(\tilde{h} - \tilde{h}_\infty) dy + \int_0^{\delta_t} \frac{\partial(\bar{\rho}\tilde{u}\tilde{h}_\infty)}{\partial x} dy = \int_0^{\delta_t} \frac{\partial(\bar{\rho}\tilde{u}\tilde{h})}{\partial x} dy \tag{A.6}$$

The first term on the left-hand side of Eq. (A.2) can be expressed using Eq. (A.6) in the following manner:

$$\frac{d}{dx}\int_0^{\delta_t} \bar{\rho}\tilde{u}(\tilde{h} - \tilde{h}_\infty) dy + \int_0^{\delta_t} \frac{\partial(\bar{\rho}\tilde{u}\tilde{h}_\infty)}{\partial x} dy + \bar{\rho}_{\delta_t}\tilde{v}_{\delta_t}\tilde{h}_{\delta_t} = \bar{q}_w + \int_0^{\delta_t} \overline{\dot{\omega}_T} dy \tag{A.7}$$

Using the chain rule for the second term on the left-hand side of Eq. (A.7) provides:

$$\frac{d}{dx}\int_0^{\delta_t}\overline{\rho}\tilde{u}\left(\tilde{h}-\tilde{h}_\infty\right)dy+\tilde{h}_\infty\int_0^{\delta_t}\frac{\partial(\overline{\rho}\tilde{u})}{\partial x}dy + \frac{d\tilde{h}_\infty}{dx}\int_0^{\delta_t}(\overline{\rho}\tilde{u})dy+\overline{\rho}_{\delta_t}\tilde{v}_{\delta_t}\tilde{h}_{\delta_t}=\overline{q}_w+\int_0^{\delta_t}\overline{\dot{\omega}_T}dy \tag{A.8}$$

The steady-state mass conservation equation $\partial(\bar{\rho}\tilde{u})/\partial x+\partial(\bar{\rho}\tilde{v})/\partial y=0$ can be used to rewrite Eq. (A.8) as:

$$\frac{d}{dx}\int_0^{\delta_t}\overline{\rho}\tilde{u}\left(\tilde{h}-\tilde{h}_\infty\right)dy-\tilde{h}_\infty\int_0^{\delta_t}\frac{\partial(\overline{\rho}\tilde{v})}{\partial x}dy + \frac{d\tilde{h}_\infty}{dx}\int_0^{\delta_t}(\overline{\rho}\tilde{u})dy+\overline{\rho}_{\delta_t}\tilde{v}_{\delta_t}\tilde{h}_{\delta_t}=\overline{q}_w+\int_0^{\delta_t}\overline{\dot{\omega}_T}dy \tag{A.9}$$

Eq. (A.9) leads to:

$$\frac{d}{dx}\int_0^{\delta_t}\overline{\rho}\tilde{u}\left(\tilde{h}-\tilde{h}_\infty\right)dy-\overline{\rho}_{\delta_t}\tilde{v}_{\delta_t}\tilde{h}_\infty+\frac{d\tilde{h}_\infty}{dx}\int_0^{\delta_t}(\overline{\rho}\tilde{u})dy + \overline{\rho}_{\delta_t}\tilde{v}_{\delta_t}\tilde{h}_{\delta_t}=\overline{q}_w+\int_0^{\delta_t}\overline{\dot{\omega}_T}dy \tag{A.10}$$

Using $\tilde{h}_{\delta_t}=\tilde{h}_\infty$ in Eq. (A.10) gives rise to:

$$\frac{d}{dx}\int_0^{\delta_t}\bar{\rho}\tilde{u}(\tilde{h}-\tilde{h}_\infty)dy+\frac{d\tilde{h}_\infty}{dx}\int_0^{\delta_t}(\bar{\rho}\tilde{u})dy=\bar{q}_w+\int_0^{\delta_t}\overline{\dot{\omega}_T}dy \tag{A.11}$$

References

[1] IEA, International Energy Agency (IEA) - World Energy Outlook 2015, Inter. Energy Agency, France, 2015.

[2] M. Rimann, C. Jainski, M. Mann, A. Dreizler, Flame-flow interaction in premixed turbulent flames during transient head-on quenching, Flow, Turbul. Combust. 98 (2017) 1025–1038, doi:10.1007/s10494-016-9795-5.

[3] C. Jainski, M. Rimann, B. Böhm, A. Dreizler, Experimental investigation of flame surface density and mean reaction rate during flame-wall interaction, Proc. Combust. Inst. 36 (2017) 1827–1834, doi:10.1016/j.proci.2016.07.113. https://linkinghub.elsevier.com/retrieve/pii/S1540748916303716

[4] C. Jainski, M. Rimann, B. Böhm, J. Janicka, A. Dreizler, Sidewall quenching of atmospheric laminar premixed flames studied by laser-based diagnostics, Combust. Flame 183 (2017) 271–282, doi:10.1016/j.combustflame.2017.05.020. https://linkinghub.elsevier.com/retrieve/pii/S0010218017301955

[5] T.J. Poinsot, D.C. Haworth, G. Bruneaux, Direct simulation and modeling of flame-wall interaction for premixed turbulent combustion, Combust Flame 95 (1993) 118–132, doi:10.1016/0010-2180(93)90056-9. https://linkinghub.elsevier.com/retrieve/pii/0010218093900569

[6] J. Lai, N. Chakraborty, A priori direct numerical simulation modeling of scalar dissipation rate transport in head-on quenching of turbulent premixed flames, Combust. Sci. Technol. 188 (2016) 1440–1471, doi:10.1080/00102202.2016.1195823.

[7] J. Lai, N. Chakraborty, Effects of Lewis number on head on quenching of turbulent premixed flames: a direct numerical simulation analysis, Flow, Turbul. Combust. 96 (2016) 279–308, doi:10.1007/s10494-015-9629-x.

[8] J. Lai, N. Chakraborty, A. Lipatnikov, Statistical behaviour of vorticity and enstrophy transport in head-on quenching of turbulent premixed flames, Eur. J. Mech. - B/Fluids 65 (2017) 384–397, doi:10.1016/j.euromechflu.2016.10.013. https://linkinghub.elsevier.com/retrieve/pii/S0997754616301625

[9] J. Lai, A. Moody, N. Chakraborty, Turbulent kinetic energy transport in head-on quenching of turbulent premixed flames in the context of reynolds averaged Navier Stokes simulations, Fuel 199 (2017) 456–477, doi:10.1016/j.fuel.2017.02.091. https://linkinghub.elsevier.com/retrieve/pii/S0016236117302430

[10] J. Lai, D. Alwazzan, N. Chakraborty, Turbulent scalar flux transport in head-on quenching of turbulent premixed flames: a direct numerical simulations approach to assess models for Reynolds averaged Navier Stokes simulations, J. Turbul. 18 (2017) 1033–1066, doi:10.1080/14685248.2017.1353218.

[11] J. Lai, M. Klein, N. Chakraborty, Direct numerical simulation of head-on quenching of statistically planar turbulent premixed methane-air flames using a detailed chemical mechanism, Flow, Turbul. Combust. 101 (2018) 1073–1091, doi:10.1007/s10494-018-9907-5.

[12] U. Ahmed, N.A.K. Doan, J. Lai, M. Klein, N. Chakraborty, N. Swaminathan, Multiscale analysis of head-on quenching premixed turbulent flames, Phys. Fluids 30 (2018) 105102, doi:10.1063/1.5047061.

[13] U. Ahmed, A.L. Pillai, N. Chakraborty, R. Kurose, Statistical behavior of turbulent kinetic energy transport in boundary layer flashback of hydrogen-rich premixed combustion, Phys. Rev. Fluids 4 (2019) 103201, doi:10.1103/PhysRevFluids.4.103201.

[14] U. Ahmed, A.L. Pillai, N. Chakraborty, R. Kurose, Surface density function evolution and the influence of strain rates during turbulent boundary layer flashback of hydrogen-rich premixed combustion, Phys. Fluids 32 (2020) 055112, doi:10.1063/5.0004850.

[15] U. Ahmed, N. Chakraborty, M. Klein, Assessment of Bray Moss Libby formulation for premixed flame-wall interaction within turbulent boundary layers: influence of flow configuration, Combust. Flame 233 (2021) 111575, doi:10.1016/j.combustflame.2021.111575. https://linkinghub.elsevier.com/retrieve/pii/S0010218021003187

[16] U. Ahmed, N. Chakraborty, M. Klein, Scalar gradient and strain rate statistics in oblique premixed flame-wall interaction within turbulent channel flows, Flow, Turbul. Combust. 106 (2021) 701–732, doi:10.1007/s10494-020-00169-3.

[17] R. Palulli, M. Talei, R.L. Gordon, Unsteady flame-wall interaction: impact on co emission and wall heat flux, Combust. Flame 207 (2019) 406–416, doi:10.1016/j.combustflame.2019.06.012. https://www.sciencedirect.com/science/article/pii/S0010218019302718

[18] B. Jiang, R.L. Gordon, M. Talei, Head-on quenching of laminar premixed methane flames diluted with hot combustion products, Proc. Combust. Inst. 37 (4) (2019) 5095–5103, doi:10.1016/j.proci.2018.07.120. https://www.sciencedirect.com/science/article/pii/S1540748918305388

[19] B. Jiang, D. Brouzet, M. Talei, R.L. Gordon, Q. Cazeres, B. Cuenot, Turbulent flame-wall interactions for flames diluted by hot combustion products, Combust. Flame 230 (2021) 111432, doi:10.1016/j.combustflame.2021.111432. https://www.sciencedirect.com/science/article/pii/S0010218021001711

[20] P. Zhao, L. Wang, N. Chakraborty, Analysis of the flame-wall interaction in premixed turbulent combustion, J. Fluid Mech. 848 (2018) 193–218, doi:10.1017/jfm.2018.356. https://www.cambridge.org/core/product/identifier/S0022112018003567/type/journal_article

[21] G. Bruneaux, K. Akselvoll, T. Poinsot, J.H. Ferziger, Flame-wall interaction simulation in a turbulent channel flow, Combust. Flame 107 (1996) 27–36, doi:10.1016/0010-2180(95)00263-4. https://linkinghub.elsevier.com/retrieve/pii/0010218095002634

[22] T. Alshaalan, C.J. Rutland, Wall heat flux in turbulent premixed reacting flow, Combust. Sci. Technol. 174 (2002) 135–165, doi:10.1080/713712913.

[23] A. Gruber, R. Sankaran, E.R. Hawkes, J.H. Chen, Turbulent flame-wall interaction: a direct numerical simulation study, J. Fluid Mech. 658 (2010) 5–32, doi:10.1017/S0022112010001278. https://www.cambridge.org/core/product/identifier/S0022112010001278/type/journal_article

[24] I. Konstantinou, U. Ahmed, N. Chakraborty, Effects of fuel Lewis number on the near-wall dynamics for statistically planar turbulent premixed flames impinging on inert cold walls, Combust. Sci. Technol. 193 (2021) 235–265, doi:10.1080/00102202.2020.1799201.

[25] J. Sellmann, J. Lai, A.M. Kempf, N. Chakraborty, Flame surface density based modelling of head-on quenching of turbulent premixed flames, Proc. Combust. Inst. 36 (2017) 1817–1825, doi:10.1016/j.proci.2016.07.114. https://linkinghub.elsevier.com/retrieve/pii/S1540748916303728

[26] P. Zhao, L. Wang, N. Chakraborty, Strain rate and flame orientation statistics in the near-wall region for turbulent flame-wall interaction, Combust. Theor. Model. 22 (2018) 921–938, doi:10.1080/13647830.2018.1465598.

[27] T.M. Alshaalan, C.J. Rutland, Turbulence, scalar transport, and reaction rates in flame-wall interaction, Symp. (Int.) Combust. 27 (1998) 793–799, doi:10.1016/S0082-0784(98)80474-8.

[28] P. Zhao, L. Wang, N. Chakraborty, Effects of the cold wall boundary on the flame structure and flame speed in premixed turbulent combustion, Proc. Combust. Inst. 38 (2021) 2967–2976, doi:10.1016/j.proci.2020.06.214. https://linkinghub.elsevier.com/retrieve/pii/S1540748920303060

[29] G. Bruneaux, T. Poinsot, J.H. Ferziger, Premixed flame-wall interaction in a turbulent channel flow: budget for the flame surface density evolution equation and modelling, J. Fluid Mech. 349 (1997) 191–219, doi:10.1017/S0022112097006769. https://www.cambridge.org/core/product/identifier/S0022112097006769/type/journal_article

[30] A. Bejan, Convection Heat Transfer, John Wiley and Sons, Ltd, 2013, doi:10.1002/9781118671627.

[31] T. Poinsot, D. Veynante, Theoretical Numerical Combustion, vol. 3, 2012.

[32] R.D. Moser, J. Kim, N.N. Mansour, DNS of turbulent channel flow up to Re_τ = 590, Phys. Fluids 11 (1999) 943–945, doi:10.1063/1.869966.

[33] P. Zhao, L. Wang, N. Chakraborty, Vectorial structure of the near-wall premixed flame, Phys. Rev. Fluids 4 (2019) 063203, doi:10.1103/PhysRevFluids.4.063203.

[34] T.D. Dunstan, N. Swaminathan, K.N. Bray, R.S. Cant, Geometrical properties and turbulent flame speed measurements in stationary premixed V-flames using direct numerical simulation, Flow, Turbul. Combust. 87 (2011) 237–259, doi:10.1007/s10494-010-9284-1.

[35] C.S. Yoo, H.G. Im, Characteristic boundary conditions for simulations of compressible reacting flows with multi-dimensional, viscous and reaction effects, Combust. Theor. Model. 11 (2007) 259–286, doi:10.1080/13647830600898995.

[36] H. Schlichting, K. Gersten, Boundary-Layer Theory, Springer Berlin Heidelberg, 2017, doi:10.1007/978-3-662-52919-5.

[37] R. Rasool, M. Klein, N. Chakraborty, Flame surface density based mean reaction rate closure for reynolds averaged Navier Stokes methodology in turbulent premixed bunsen flames with non-unity Lewis number, Combust. Flame 239 (2022) 111766, doi:10.1016/j.combustflame.2021.111766. A dedication to Professor Kenneth Noel Corbett Bray, https://www.sciencedirect.com/science/article/pii/S0010218021005095

[38] F. Ammouri, J. Taine, Measurement of wall conductive heat flux in turbulent gas flow by laser beam deflection, Int. J. Heat Mass Transf. 37 (12) (1994) 1759–1771, doi:10.1016/0017-9310(94)90065-5. https://www.sciencedirect.com/science/article/pii/0017931094900655

[39] A.O. Ojo, D. Escofet-Martin, C. Abram, B. Fond, B. Peterson, Precise surface temperature measurements at kHz-rates using phosphor thermometry to study flame-wall interactions in narrow passages, Combust. Flame 240 (2022) 111984, doi:10.1016/j.combustflame.2022.111984. https://www.sciencedirect.com/science/article/pii/S0010218022000037

[40] D. Escofet-Martin, A. Ojo, N. Mecker, M. Linne, B. Peterson, Simultaneous 1D hybrid fs/ps rotational CARS, phosphor thermometry, and CH* imaging to study transient near-wall heat transfer processes, Proc. Combust. Inst. 38 (1) (2021) 1579–1587, doi:10.1016/j.proci.2020.06.097. https://www.sciencedirect.com/science/article/pii/S1540748920301565